When less is more: the truncation of the optimal filter to reconstruct events in X-IFU/Athena-like TES detectors

M.T. Ceballos[a], N. Cardiel[b], B. Cobo[a], P. Peille[c], S.J. Smith[d], M. C. Witthoeft[d,e], and M.S. Durkin[f,g]

[a]Instituto de Fïsica de Cantabria, CSIC-UC, Avda Los Castros s/n, E-39005 Santander, Spain
[b]Departamento de Física de la Tierra y Astrofísica, Universidad Complutense de Madrid, Plaza Ciencias 1, E-28040 Madrid, Spain
[c]CNES, 18 Av. Edouard Belin, 31401 Toulouse Cedex 9, France
[d]NASA Goddard Space Flight Centre, USA
[e]ADNET Systems, Inc, Bethesda, MD, USA
[f]National Institute of Standards and Technology, Boulder, CO, USA
[g]Department of Physics, University of Colorado, Boulder, CO, USA

ABSTRACT

The X-ray Integral Field Unit (X-IFU) instrument to be on board the future ESA mission Athena X-ray Observatory is a cryogenic micro-calorimeter array of Transition Edge Sensor (TES) detectors aimed at providing spatially resolved high-resolution spectroscopy. As a part of the on-board Event Processor (EP), the reconstruction software will provide the energy, spatial location and arrival time of the incoming X-ray photons hitting the detector and inducing current pulses on it. Being the standard optimal filtering technique the chosen baseline reconstruction algorithm, a particular modification of this technique based on a truncation of the filter in the Time Domain (equivalent to *0-padding* the pulse signal) was previously studied on simulated data, proving a better energy resolution results at a lower computational cost. However, the *0-padding* technique also showed a larger sensitivity to instrumental conditions, making essential the analysis of its behaviour over real laboratory data. A comparative analysis of X-IFU-like TES laboratory data from NASA and NIST (at different instrumental conditions) with both the *0-padding* filter and the standard optimal filters reconstruction shows that, once the corrections for the baseline drift and the jitter (phase introduced by the sampling rate) have been performed, the resolution values obtained using *0-padding* are systematically lower than those of the standard filter of the same length and comparable or even lower to the values provided by the full-length filter. The shorter length of the *0-padding* filter would be an additional benefit, reducing the computational cost of the reconstruction process.

Keywords: Athena, X-ray Integral Field Unit, X-ray spectroscopy, space telescopes, instrumentation, reconstruction methods, performance analysis

1. INTRODUCTION

The X-ray Integral Field Unit (X-IFU)[1] will be one of the two instruments on-board the ESA's *Athena* mission.[2] It is a high-resolution cryogenic imaging spectrometer in the 0.2-12 keV band that will provide unprecedented spectral resolution (2.5 eV at 7 keV). The X-IFU Focal Plane will contain a large array of Transition Edge Sensors (TES) in groups of several tens of TES per readout channel considering a Time Division Multiplexing (TDM) scheme.[3] The on-board Event Processor (EP)[4] hardware performs the reconstruction of the detected events caused by the impact of the X-ray photons, to estimate their energy and arrival time and also their spatial location (based on impact pixel).

Further author information: (Send correspondence to M.T. Ceballos)
M.T. Ceballos: E-mail: ceballos@ifca.unican.es

The main challenge of the event processing is to get the best energy resolution from the photons with a reduced computational cost. Therefore, the selected algorithms to work in the EP should be optimal and capable of minimising the degradation of the energy resolution with energy due to the non-linearity of the detector.

The baseline reconstruction method for the X-IFU events is currently the optimal filtering.[5] The time stream data is digitized into records of a fixed length which are used to build the signal and noise parts of the filter. For the signal portion, the Discrete Fourier Transform (DFT) of the average of many pulse records is calculated, whereas the noise portion is built averaging the spectra of many pulse-free records. The $f = 0$ Hz bin of the DFT contains an arbitrary and slowly varying offset, so it is commonly discarded. That way, the final filter is zero summed and the signal baseline can be effectively rejected from the processing.

Working in time domain, the energy of the photon is simply proportional to the scalar product of the data pulse and an optimal filter:

$$E = k \int d(t) \cdot of(t)\ \mathrm{d}t$$

where $d(t)$ is the pulse data, $of(t)$ is the time domain expression of the optimal filter and k is the normalization factor to give E in units of energy:

$$k = \int \frac{S(f) \cdot S^*(f)}{\langle |N(f)|^2 \rangle}\ \mathrm{d}f$$

The matched filter (a normalized model pulse shape, $S(f)$) and the noise spectrum ($N(f)$) are used to initially build the optimal filter in frequency domain as:

$$of(f) = \frac{S^*(f)}{\langle |N(f)|^2 \rangle}$$

The instrument energy resolution obtained after the events reconstruction is characterized by the Full Width at Half Maximum (FWHM) of the Gaussian broadening produced by the instrumental setup (and the reconstruction algorithm) on top of the Lorentzian natural profile of the line complex.

As the average value of the filtered pulse is set to 0 ($f = 0$ Hz bin), the number of samples used in the discrete expression of the data pulse and the filter has also an impact on the final energy resolution provided by the optimal filter.[6] The resolution improves with the record length, but at the expense of a larger computational cost.

Aiming at a reduction in the number of computing operations to be done on board, in a previous work[7] we explored the application of a variation of the optimal filter technique, consisting on a truncation of the full-length optimal filter in the time domain (equivalent to *0-padding* the data pulse). We then compared this *0-padding* approach with the results obtained with the full-length version of the optimal filter, and also with a short optimal filter built from a shorter template. The study was performed over synthetic data simulated with the X-IFU official simulator XIFUSIM.[8] The main conclusion of this test was the better performance shown by the *0-padding* technique when compared not only with an optimal filter of the same length but also with a twice-as-long optimal filter that is the baseline filter for the high resolution events.

However, the analysis also revealed the higher sensitivity of the *0-padding* filter to the varying instrumental conditions, in particular the bath temperature causing baseline drifts. At that point a test of this method over the real laboratory data proved essential before considering *0-padding* as a real alternative to the current baseline reconstruction algorithm.

In this work we present the results (in terms of energy resolution) obtained applying the *0-padding* filter to TES data from Goddard Space Flight Center (GSFC) and National Institute of Standards and Technology (NIST) laboratories. We compared these results with those provided by the application of a full optimal filter (baseline method at these laboratories) and also of a shorter version of it (equal in length to the *0-padding* filter).

Section 2 presents the data used in the analysis; section 3 shows the three different filters used for the reconstruction; sections 4 and 5 describe the corrections applied to the data and the fitting routines used to retrieve the energy resolution respectively, and section 6 presents the results of the filter comparative.

2. THE LABORATORY DATA

The data analysed in this work belong to three datasets with different X-ray line complexes, count rates and bath temperature drifts:

- **10Jan2020** (GSFC): initial dataset with several line complexes and 8x32 channels in the TES.
- **LargeTdrift** (NIST): two column measurement (2x32 channels) taken with the NASA LPA array at NIST in a cryostat that exhibits much larger drift. This dataset was used to test *0-padding* reconstruction under conditions of worse temperature stability.
- **30Sep2020** (GSFC): lower count rate dataset of line complex MnKα (8x32 channels), to avoid an additional effect on the energy resolution caused by a possible imperfect removal of crosstalk events which could contaminate the Mn complex.

The typical single pulses of the different datasets are displayed in Figure 1. As it can be seen, they differ both in the total length of the data record and in the pre-trigger length (data signal before the rising of the pulse).

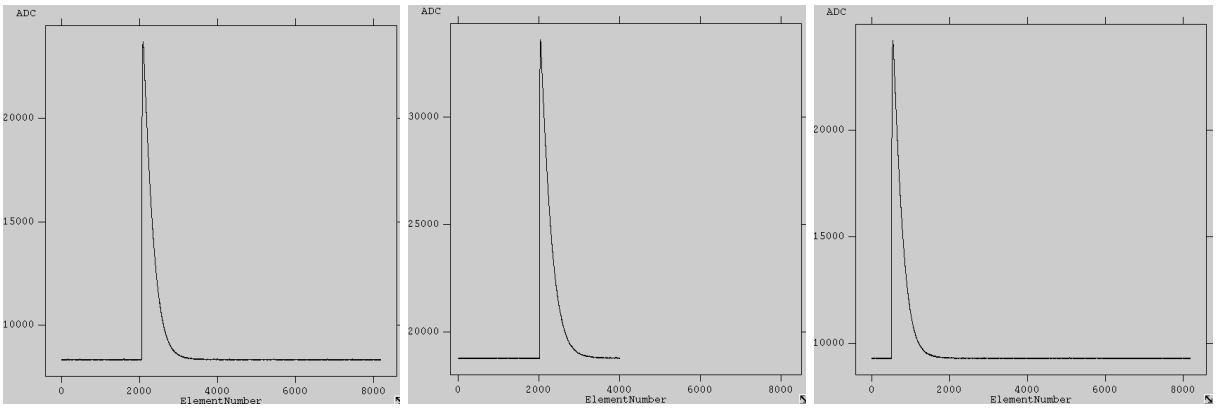

Figure 1. Data records showing typical pulses for each dataset: 10Jan2020 (left), LargeTdrift (middle), 30Sep2020 (right). In the X axis, the time in samples for a sampling rate of 156.25 Hz and in the Y axis the intensity of the pulse in arbitrary units.

3. FILTER CONSTRUCTION

The pulse template accounting for the signal part of the optimal filter is built by averaging the largest number of isolated and (as much as possible) monochromatic Mn Kα pulses (5.9 keV). For this, the records with multiple pulses were discarded as well as the pulses with pulse heights (and thus, energies) out of the range of those of the Mn Kα complex. In addition, the records contaminated by crosstalk events (events produced by a close-in-time impact of another X-ray photon in a different pixel of the same TDM reading column) were also eliminated from the analysis.

To obtain the noise spectrum, we selected the *cleanest* set of noise records (free from instrumental artifacts or undesirable effects), removing those giving the largest residuals with respect to the mean noise spectrum.

With the pulse template and the average noise spectrum, three distinct optimal filters are built using different pulse lengths in the pulse template or truncating an existing long filter in the time domain.

The three types of filters we have used in the analysis of all the datasets are:

- FULL: the pulse template is obtained using the maximum length permitted by the data records, including the pre-trigger signal (see Table 1)
- SHORT: the pulse template is built using pulses only half the length of the record (to save computational resources)
- ***0-padding***: the optimal filter is built in the same manner as the FULL filter, but once in the time domain, its length is truncated to half the value of the FULL filter length (thus, equivalent to the length of the SHORT filter but with a different construction technique).

DATA	Pre-trigger	FULL	SHORT	0-padding
10Jan2020	2000	8000	4096	4096
LargeTdrift	1000	2900	1450	1450
30Sep2020	450	8000	4096	4096

Table 1. Filters pre-trigger lengths and total lengths (in samples, for a sampling rate of 156.25 kHz.)

4. DATA CORRECTIONS

Once the data pulses have been filtered with the three different filters described in section 3, reconstructed energies must be corrected for the consequences of the instrumental variations produced during data acquisition. The most important effects are produced by the baseline drift due to instabilities in the bath temperature of the TES setup, and by the offset between the physical/real arrival time of the photon and the measured/digitized arrival time (*jitter*).

The correction is performed by a simple cross-correlation technique where data (reconstructed energies) in a moving window are continuously compared with the average histogram of the full data distribution. This way it is possible to determine any potential energy offset with time (coupled to the baseline drift) or phase (jitter).

An example of the correction for one of the pixels in 10Jan2020 dataset can be seen in Figure 2.

The final additional correction that must be applied to the data is the energy calibration. The optimal filter technique assumes that all the pulses are re-scaled versions of a model one, but the non linear behaviour of the TES produces small offsets in the reconstructed energy once the data is out of the energy of the filter. As the dispersion in energy of the reconstructed events is small in this case (we are using the MnKα complex to calculate the energy resolution), we do a local energy calibration using the three peaks of MnKα_1, MnKα_2 and MnKβ. We simply fit the data histograms with a double Gaussian for MnKα and a single Gaussian for MnKβ. The local calibration curve is just then the degree 2 polynomial fit to the location of the Gaussian centres.

5. FITTING

Due to the TES response, the measured MnKα complex is a convolution of the natural Lorentzian profile of the lines and the Gaussian broadening produced by the instrumental setup. In addition, the reconstruction algorithm can increase the latter, being important to find the best compromise between minimization of this effect and reduction of the computational cost.

The result of this Lorentzian-Gaussian convolution is called a Voigt profile and it is the model that we have used to fit the corrected-calibrated energy distribution of MnKα data.

The data histograms have been fitted using *AstroPy*[9,10] Fitting module (using `LevMarLSQFitter`). The models used for the MnKα are 8 *Voigt* profiles where the *Voigt* relative intensities of the lines are kept tied, the

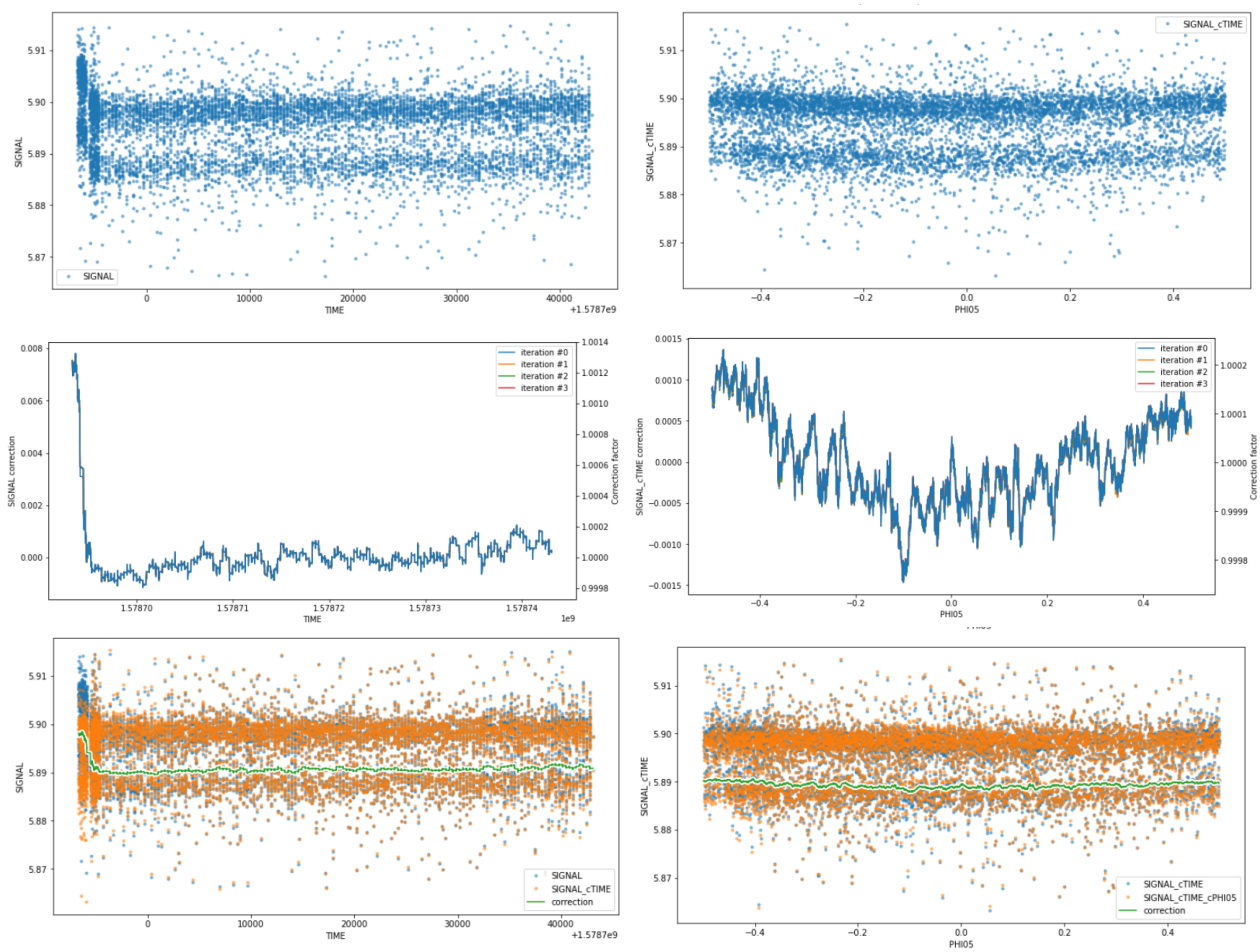

Figure 2. TIME (left column) and JITTER (right column) corrections of MnKα complex pulses. Top: reconstructed Pulse Height vs TIME/JITTER; middle: correction curves; bottom: corrected distributions (orange)

distance of the line centres are also tied, the *Lorentzian* FWHMs are kept fixed (according to lab data values[11]) and the Gaussian broadening is a free parameter, the same for all the lines. It is precisely the FWHM of this Gaussian broadening the figure of merit to quantify the energy resolution of the detector.

For the *AstroPy* fitting procedure, different weights for the `LevmarLSQFitter` call have been tested:

* **iSig:** histogram bins are weighted by the number of counts N within each bin ($\sigma^2 = N$)
* **SN:** histogram bins are weighted by the Signal-to-Noise ratio in the bin ($\sigma^2 = \frac{1}{\sqrt{N}}$)
* **None:** no weight is applied ($\sigma^2 = 1$)

The *iSig* options follows the approach suggested by Fowler (2014)[12] as the best approximation to the maximum likelihood fit (Neyman's χ^2 plus iteration). *SN* weights are also applied through an iterative process, which should remove any bias in the histogram fitting process.

The other important parameter when dealing with histograms fitting is the number of bins. After studying the dependency of the FWHM values obtained for different number of bins, we have chosen a value of 3000 bins (for a total number of 8000 data points spread in the fitted energy range), a number where this dependency becomes stable.

6. RESULTS

The resulting energy resolution for all the pixels in the different datasets, for the three filters described in section 3 and the three different weights explained in section 5 are shown in Figure 3.

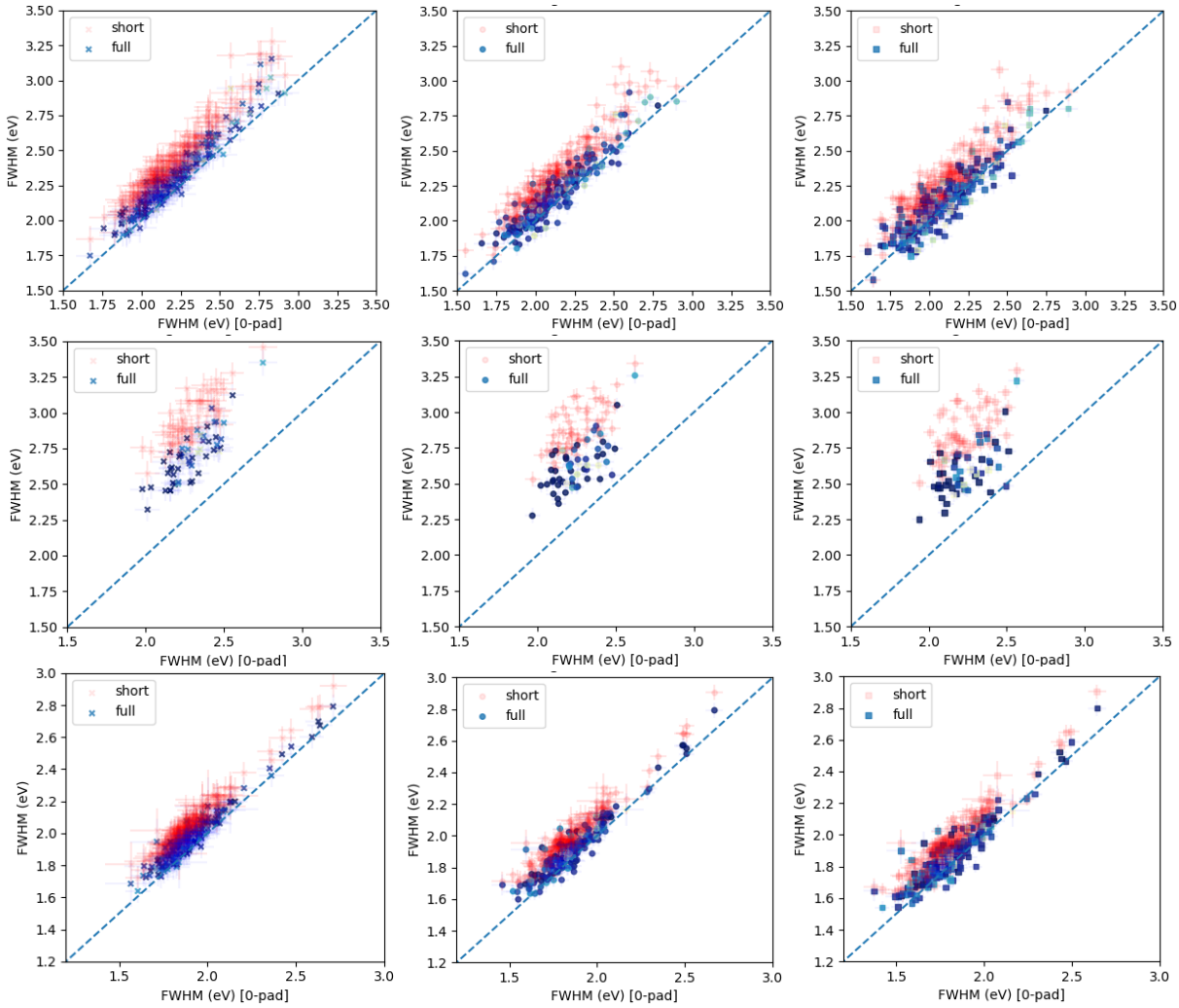

Figure 3. Comparison of resolution values for FULL filter (blue) and SHORT filter (red) in Y axis vs those from the *0-padding* filter reconstruction (X-axis) for datasets 10Jan2020 (top), LargeTdrift (middle) and 30Sep2020 (bottom), and three different weights in the minimization process, *iSig* (left), *None* (center) and *SN* (right).

For all the datasets (with different instrumental stability conditions and crosstalk levels) and for the three different weights applied to the histogram fitting process, the *0-padding* filter shows better energy resolution values not only in comparison with the other filter of equal length (SHORT filter) but also with the FULL length filter, with the additional benefit of a reduced computational cost. However, since it is a truncation of the FULL filter, it is not zero-summed anymore and this could make it more sensitive to fluctuations of the signal baseline during data acquisition, as it was observed with previous tests done on synthetic data.[7] This sensitivity to instrumental drifts can be though removed with the corrections for the baseline drift and jitter presented in section 4.

7. CONCLUSIONS

A variation of the classical *optimal filter* algorithm has been proposed as the method to retrieve the energy of the photons detected by a TES device like the one to be on board the *Athena* mission.

This variation (*0-padding*) consists in a truncation of the optimal filter in its time domain expression. When compared with an optimal filter of the same length (built from a shorter template instead of truncating the filter) it shows a much better performance. The resolution values provided are similar or slightly better even than those resulting from the application of a double-length optimal filter, with the additional benefit of a reduced computational cost.

Provided the corrections for the baseline drift and jitter can be performed, the *0-padding* filter results in the best option to reconstruct the energy of the X-ray photons arriving to the TES detector. This is a very promising result as the shorter length of *0-padding* filters would require less computational resources (very important for onboard processing) and could also let sources with larger count rates be analyzed in high resolution.

ACKNOWLEDGMENTS

M.T. Ceballos, N. Cardiel and B. Cobo acknowledge grant RTI2018-096686-B-C21 funded by MCIN/AEI/ 10.13039/501100011033 and by "ERDF A way of making Europe"

REFERENCES

[1] Barret, D., Trong, T. L., den Herder, J.-W., Piro, L., Cappi, M., Houvelin, J., Kelley, R., Mas-Hesse, J. M., Mitsuda, K., Paltani, S., Rauw, G., Rozanska, A., Wilms, J., Bandler, S., Barbera, M., Barcons, X., Bozzo, E., Ceballos, M. T., Charles, I., Costantini, E., Decourchelle, A., den Hartog, R., Duband, L., Duval, J.-M., Fiore, F., Gatti, F., Goldwurm, A., Jackson, B., Jonker, P., Kilbourne, C., Macculi, C., Mendez, M., Molendi, S., Orleanski, P., Pajot, F., Pointecouteau, E., Porter, F., Pratt, G. W., Prêle, D., Ravera, L., Sato, K., Schaye, J., Shinozaki, K., Thibert, T., Valenziano, L., Valette, V., Vink, J., Webb, N., Wise, M., Yamasaki, N., Douchin, F., Mesnager, J.-M., Pontet, B., Pradines, A., Branduardi-Raymont, G., Bulbul, E., Dadina, M., Ettori, S., Finoguenov, A., Fukazawa, Y., Janiuk, A., Kaastra, J., Mazzotta, P., Miller, J., Miniutti, G., Naze, Y., Nicastro, F., Scioritino, S., Simonescu, A., Torrejon, J. M., Frezouls, B., Geoffray, H., Peille, P., Aicardi, C., André, J., Daniel, C., Clénet, A., Etcheverry, C., Gloaguen, E., Hervet, G., Jolly, A., Ledot, A., Paillet, I., Schmisser, R., Vella, B., Damery, J.-C., Boyce, K., Dipirro, M., Lotti, S., Schwander, D., Smith, S., Leeuwen, B.-J. V., van Weers, H., Clerc, N., Cobo, B., Dauser, T., Kirsch, C., Cucchetti, E., Eckart, M., Ferrando, P., and Natalucci, L., "The ATHENA X-ray Integral Field Unit (X-IFU)," in [*Space Telescopes and Instrumentation 2018: Ultraviolet to Gamma Ray*], den Herder, J.-W. A., Nikzad, S., and Nakazawa, K., eds., **10699**, 324 – 338, International Society for Optics and Photonics, SPIE (2018). 1

[2] Nandra, K., Barret, D., Barcons, X., Fabian, A., Herder, J.-W. d., Piro, L., Watson, M., Adami, C., Aird, J., Afonso, J. M., Alexander, D., Argiroffi, C., Amati, L., Arnaud, M., Atteia, J.-L., Audard, M., Badenes, C., Ballet, J., Ballo, L., Bamba, A., Bhardwaj, A., Battistelli, E. S., Becker, W., De Becker, M., Behar, E., Bianchi, S., Biffi, V., Bîrzan, L., Bocchino, F., Bogdanov, S., Boirin, L., Boller, T., Borgani, S., Borm, K., Bouché, N., Bourdin, H., Bower, R., Braito, V., Branchini, E., Branduardi-Raymont, G., Bregman, J., Brenneman, L., Brightman, M., Brüggen, M., Buchner, J., Bulbul, E., Brusa, M., Bursa, M., Caccianiga, A., Cackett, E., Campana, S., Cappelluti, N., Cappi, M., Carrera, F., Ceballos, M., Christensen, F., Chu, Y.-H., Churazov, E., Clerc, N., Corbel, S., Corral, A., Comastri, A., Costantini, E., Croston, J., Dadina, M., D'Ai, A., Decourchelle, A., Della Ceca, R., Dennerl, K., Dolag, K., Done, C., Dovciak, M., Drake, J., Eckert, D., Edge, A., Ettori, S., Ezoe, Y., Feigelson, E., Fender, R., Feruglio, C., Finoguenov, A., Fiore, F., Galeazzi, M., Gallagher, S., Gandhi, P., Gaspari, M., Gastaldello, F., Georgakakis, A., Georgantopoulos, I., Gilfanov, M., Gitti, M., Gladstone, R., Goosmann, R., Gosset, E., Grosso, N., Guedel, M., Guerrero, M., Haberl, F., Hardcastle, M., Heinz, S., Herrero, A. A., Hervé, A., Holmstrom, M., Iwasawa, K., Jonker, P., Kaastra, J., Kara, E., Karas, V., Kastner, J., King, A., Kosenko, D., Koutroumpa, D., Kraft, R., Kreykenbohm, I., Lallement, R., Lanzuisi, G., Lee, J., Lemoine-Goumard, M., Lobban, A., Lodato, G., Lovisari, L., Lotti, S., McCharthy, I., McNamara, B., Maggio, A., Maiolino, R., De Marco, B., de Martino, D., Mateos, S., Matt, G., Maughan, B., Mazzotta, P., Mendez, M., Merloni, A., Micela, G., Miceli, M., Mignani, R., Miller, J., Miniutti, G., Molendi, S., Montez, R., Moretti, A., Motch, C., Nazé, Y., Nevalainen, J., Nicastro, F., Nulsen, P., Ohashi, T., O'Brien, P., Osborne, J., Oskinova, L., Pacaud, F., Paerels, F., Page, M., Papadakis, I., Pareschi, G., Petre, R., Petrucci, P.-O., Piconcelli, E., Pillitteri, I., Pinto, C., de Plaa, J., Pointecouteau, E., Ponman, T., Ponti, G., Porquet, D., Pounds, K., Pratt, G., Predehl, P., Proga, D., Psaltis, D., Rafferty,

D., Ramos-Ceja, M., Ranalli, P., Rasia, E., Rau, A., Rauw, G., Rea, N., Read, A., Reeves, J., Reiprich, T., Renaud, M., Reynolds, C., Risaliti, G., Rodriguez, J., Hidalgo, P. R., Roncarelli, M., Rosario, D., Rossetti, M., Rozanska, A., Rovilos, E., Salvaterra, R., Salvato, M., Di Salvo, T., Sanders, J., Sanz-Forcada, J., Schawinski, K., Schaye, J., Schwope, A., Sciortino, S., Severgnini, P., Shankar, F., Sijacki, D., Sim, S., Schmid, C., Smith, R., Steiner, A., Stelzer, B., Stewart, G., Strohmayer, T., Strüder, L., Sun, M., Takei, Y., Tatischeff, V., Tiengo, A., Tombesi, F., Trinchieri, G., Tsuru, T. G., Ud-Doula, A., Ursino, E., Valencic, L., Vanzella, E., Vaughan, S., Vignali, C., Vink, J., Vito, F., Volonteri, M., Wang, D., Webb, N., Willingale, R., Wilms, J., Wise, M., Worrall, D., Young, A., Zampieri, L., Zand, J. I., Zane, S., Zezas, A., Zhang, Y., and Zhuravleva, I., "The hot and energetic universe: A white paper presenting the science theme motivating the athena+ mission," (2013). 1

[3] Durkin, M., Adams, J. S., Bandler, S. R., Chervenak, J. A., Chaudhuri, S., Dawson, C. S., Denison, E. V., Doriese, W. B., Duff, S. M., Finkbeiner, F. M., FitzGerald, C. T., Fowler, J. W., Gard, J. D., Hilton, G. C., Irwin, K. D., Joe, Y. I., Kelley, R. L., Kilbourne, C. A., Miniussi, A. R., Morgan, K. M., O'Neil, G. C., Pappas, C. G., Porter, F. S., Reintsema, C. D., Rudman, D. A., Sakai, K., Smith, S. J., Stevens, R. W., Swetz, D. S., Szypryt, P., Ullom, J. N., Vale, L. R., Wakeham, N. A., Weber, J. C., and Young, B. A., "Demonstration of athena x-ifu compatible 40-row time-division-multiplexed readout," *IEEE Transactions on Applied Superconductivity* **29**(5), 1–5 (2019). 1

[4] Ravera, L., Cara, C., Ceballos, M. T., Barcons, X., Barret, D., Clédassou, R., Clénet, A., Cobo, B., Doumayrou, E., den Hartog, R. H., van Leeuwen, B.-J., van Loon, D., Mas-Hesse, J. M., Pigot, C., and Pointecouteau, E., "The DRE: the digital readout electronics for ATHENA X-IFU," in [*Space Telescopes and Instrumentation 2014: Ultraviolet to Gamma Ray*], Takahashi, T., den Herder, J.-W. A., and Bautz, M., eds., **9144**, 1734 – 1741, International Society for Optics and Photonics, SPIE (2014). 1

[5] Szymkowiak, A. E., Kelley, R., Moseley, S. H., and Stahle, C. K., "Signal processing for microcalorimeters," *Journal of Low Temperature Physics, 93(3)* **93**, 281–285 (1993). 2

[6] Doriese, W. B., Adams, J., Hilton, G., Irwin, K., Kilbourne, C., Schima, F., and Ullom, J., "Optimal filtering, record length, and count rate in transition-edge-sensor microcalorimeters," in [*AIP Conference Proceedings*], **1185**(1), 450–453, American Institute of Physics (2009). 2

[7] Cobo, B., Cardiel, N., Ceballos, M. T., and Peille, P., "Pulse processing in TES detectors: comparative of different short filter methods based on optimal filtering: case study for Athena X-IFU," in [*Space Telescopes and Instrumentation 2020: Ultraviolet to Gamma Ray*], den Herder, J.-W. A., Nikzad, S., and Nakazawa, K., eds., **11444**, 1333 – 1344, International Society for Optics and Photonics, SPIE (2020). 2, 6

[8] Kirsch, C., Lorenz, M., Peille, P., Dauser, T., Ceballos, M. T., Cobo, B., Merino-Alonso, P. E., Cucchetti, E., Smith, S., Gottardi, L., Hartog, R. H. d., Miniussi, A., Durkin, M., Prêle, D., and Wilms, J., "The athena x-ifu instrument simulator xifusim," *Journal of Low Temperature Physics* (Mar 2022). 2

[9] Astropy Collaboration, Robitaille, T. P., Tollerud, E. J., Greenfield, P., Droettboom, M., Bray, E., Aldcroft, T., Davis, M., Ginsburg, A., Price-Whelan, A. M., Kerzendorf, W. E., Conley, A., Crighton, N., Barbary, K., Muna, D., Ferguson, H., Grollier, F., Parikh, M. M., Nair, P. H., Unther, H. M., Deil, C., Woillez, J., Conseil, S., Kramer, R., Turner, J. E. H., Singer, L., Fox, R., Weaver, B. A., Zabalza, V., Edwards, Z. I., Azalee Bostroem, K., Burke, D. J., Casey, A. R., Crawford, S. M., Dencheva, N., Ely, J., Jenness, T., Labrie, K., Lim, P. L., Pierfederici, F., Pontzen, A., Ptak, A., Refsdal, B., Servillat, M., and Streicher, O., "Astropy: A community Python package for astronomy," *Astronomy and Astrophysics* **558**, A33 (Oct. 2013). 4

[10] Astropy Collaboration, Price-Whelan, A. M., Sipőcz, B. M., Günther, H. M., Lim, P. L., Crawford, S. M., Conseil, S., Shupe, D. L., Craig, M. W., Dencheva, N., Ginsburg, A., Vand erPlas, J. T., Bradley, L. D., Pérez-Suárez, D., de Val-Borro, M., Aldcroft, T. L., Cruz, K. L., Robitaille, T. P., Tollerud, E. J., Ardelean, C., Babej, T., Bach, Y. P., Bachetti, M., Bakanov, A. V., Bamford, S. P., Barentsen, G., Barmby, P., Baumbach, A., Berry, K. L., Biscani, F., Boquien, M., Bostroem, K. A., Bouma, L. G., Brammer, G. B. andBray, E. M., Breytenbach, H., Buddelmeijer, H., Burke, D. J., Calderone, G., Cano Rodríguez, J. L., Cara, M., Cardoso, J. V. M., Cheedella, S., Copin, Y., Corrales, L., Crichton, D., D'Avella, D., Deil, C., Depagne, É., Dietrich, J. P., Donath, A., Droettboom, M., Earl, N., Erben, T., Fabbro, S., Ferreira, L. A., Finethy, T., Fox, R. T., Garrison, L. H., Gibbons, S. L. J., Goldstein, D. A., Gommers, R., Greco, J. P., Greenfield, P., Groener, A. M., Grollier, F., Hagen, A., Hirst, P., Homeier, D., Horton, A. J., Hosseinzadeh, G., Hu, L.,

Hunkeler, J. S., Ivezić, Ž., Jain, A., Jenness, T., Kanarek, G., Kendrew, S., Kern, N. S., Kerzendorf, W. E., Khvalko, A., King, J., Kirkby, D., Kulkarni, A. M., Kumar, A., Lee, A., Lenz, D., Littlefair, S. P., Ma, Z., Macleod, D. M., Mastropietro, M., McCully, C., Montagnac, S., Morris, B. M., Mueller, M., Mumford, S. J., Muna, D., Murphy, N. A., Nelson, S., Nguyen, G. H., Ninan, J. P., Nöthe, M., Ogaz, S., Oh, S., Parejko, J. K., Parley, N., Pascual, S., Patil, R., Patil, A. A., Plunkett, A. L., Prochaska, J. X., Rastogi, T., Reddy Janga, V., Sabater, J., Sakurikar, P., Seifert, M., Sherbert, L. E., Sherwood-Taylor, H., Shih, A. Y., Sick, J., Silbiger, M. T., Singanamalla, S., Singer, L. P., Sladen, P. H., Sooley, K. A., Sornarajah, S., Streicher, O., Teuben, P., Thomas, S. W., Tremblay, G. R., Turner, J. E. H., Terrón, V., van Kerkwijk, M. H., de la Vega, A., Watkins, L. L., Weaver, B. A., Whitmore, J. B., Woillez, J., Zabalza, V., and Astropy Contributors, "The Astropy Project: Building an Open-science Project and Status of the v2.0 Core Package," *Astronomical Journal* **156**, 123 (Sept. 2018). 4

[11] Eckart, M., Kilbourne, C., and Porter, F., "Instrument Calibration Report – Natural Line shapes of SXS onboard calibration sources," *ASTH-SXS-CALBD-LINEFIT – v0.2* (2016). 5

[12] Fowler, J. W., "Maximum-Likelihood Fits to Histograms for Improved Parameter Estimation," *Journal of Low Temperature Physics* **176**, 414 (Aug. 2014). 5